Journal of Materials Sciences and Applications
2019; 5(3): 44-57
http://www.aascit.org/journal/jmsa
ISSN: 2381-0998 (Print); ISSN: 2381-1005 (Online)

American Association for Science and Technology

Strain-induced Electric Effects in Condensed Matters

Yuanjie Huang

Institute of Fluid Physics, Chinese Academy of Engineering Physics, Mianyang, China

Email address
hyj201207@163.com

Citation
Yuanjie Huang. Strain-induced Electric Effects in Condensed Matters. *Journal of Materials Sciences and Applications*. Vol. 5, No. 3, 2019, pp. 44-57.

Received: April 22, 2019; **Accepted**: June 5, 2019; **Published**: June 20, 2019

Abstract: In this work, shock polarization, electric properties of dislocations and mechanical-electric coupling are investigated in condensed matters. By means of research, a new law for condensed matters was found and it was formally named as *Yuheng Zhang equation*. Utilizing this law, it is found that 1) under non-uniform strain, materials may behave as a p-n junction, exhibiting current-rectifying properties; 2) pure semiconductors with strain gradient can be utilized as a solar cell; 3) thermoelectric power or Seebeck coefficient of materials may be dominated by this law and thermal expansion (contraction); 4) this law gives a new mechanism of electron-phonon interaction; 5) an electric field always accompanies defects in materials, such as dislocations, Abrikosov vortices and so on, and their electric field and related electrical potential are given; 6) strain gradient can cause an electric polarization in dielectric materials; 7) the gravity induced electric field persists within planets including the earth; 8) this law may be the microscopic physical origin of flexoelectric effect and the flexoelectric coefficients can be derived by means of this equation; 9) microscopic theory of shock polarization, another long-standing problem in the world, may be clarified in terms of this law. In all, the newly found law may offer people new understanding of electric properties of strained materials, and may find various applications in multi-areas.

Keywords: Mechanical-electric Coupling, Dislocation, Shock Polarization, Flexoelectric Effect

1. Introduction

Deformations can generate an electrical potential difference between surfaces of deformed ionic crystals, which may be first revealed by A. V. Stepanov [1]. A similar effect, namely, shock polarization, a phenomena that an electrical potential difference appears in almost all types of samples when they are dynamically loaded, was established and has been investigated for many decades [2-7]. As for shock polarization, many people attempted to interpret it and put forward many mechanisms for different materials, such as microscopic linear ionic chain model [8] and dislocation model [9] for ionic crystals, phenomenological mechanical polarization model for plastics [10], polar molecule rotating model for polar dielectrics [11] and so on. However, the microscopic mechanism for shock polarization is still little known and is challenging.

On the other hand, dislocations have attracted much attention in recent years, because besides conventional mechanical properties they also exhibit electric properties and can detrimentally affect performances of semiconductor devices, as is revealed by experiments [12-16]. Actually, in early years electric properties of dislocations was speculated and observed in deformation processes of some crystals. For instance, electric charges are reported to accompany with dislocations during plastic deformation of materials such as sodium chloride [17, 18]. For a small angle grain boundary constructed by dislocations, experimental investigations show that it can bear charges and migrate under an external electric field [19]. Further experimental observations indicate that lattice-mismatch induced dislocations in a thin film give rise to a drastic degradation in piezoelectric constant and switched electric polarization [20]. Phenomenological analysis demonstrated that in ferroelectric films polarization varies dramatically near a dislocation and its gradient leads to suppression of polarization over several nanometers [21]. However, a detailed knowledge of dislocation on electric properties is completely lacking and the microscopic mechanism has been still unclear [22].

In this work, the related phenomena are mainly investigated in an effort to clarify their underlying microscopic physical mechanism in theory.

2. Theoretical Methods

Like the case in metals, let us consider a typical semiconductor or insulator undergoing strains. For the regions under strains, the Fermi surface for electrons may be lifted. Thus a discrepancy of Fermi surface appears between the strained and unstrained regions. The electrons in regions with higher Fermi surface tend to shift to regions with lower Fermi surface, thereby creating an electric field and an electric potential between the regions, as is shown in Figure 1. As is known, mass of electrons is much smaller than that of ions or atoms in materials, so response time scale of electrons is much shorter than that of ions or atoms. Therefore once the ions or atoms move in the materials, electrons response and approach their equilibrium state rapidly. These processes may be described by the equations,

$$\nabla E_F(\vec{r}) = q\vec{E}(\vec{r}) \tag{1}$$

$$qV_Z = E_F(\vec{r}_1) - E_F(\vec{r}_2) \tag{2}$$

where $E_F(\vec{r})$ is position dependence of Fermi surface energy, namely, chemical potential in some literatures, q is electron charge and $\vec{E}(\vec{r})$ is the yielded electric fields, V_Z is the induced electric potential. Despite that this equation first appears in reference [23], to be consistent with name of this effect, i.e. *Yuheng Zhang effect*, here Equation (1) is formally named as *Yuheng Zhang Equation*.

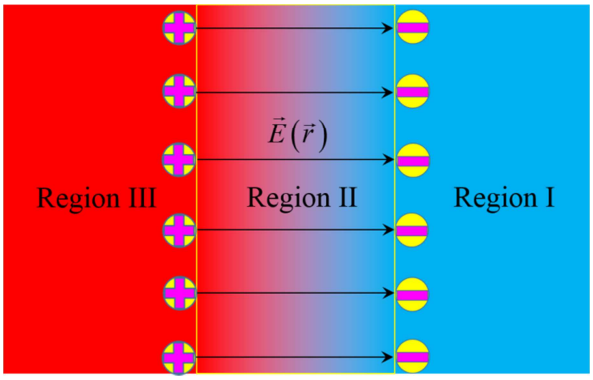

Figure 1. *Schematic diagram of an electric field caused by Yuheng Zhang effect in materials: blue zones (Region I) and red zones (Region III) denote the unstrained regions and strained regions, respectively, and color gradient zone is strain gradient regions (Region II); stuffed circles with negative sign and stuffed circles with positive sign present electrons and ions; arrows in Region II give the possible electric field.*

3. Results and Discussion

Yuheng Zhang equation may be valid for metals, semiconductors and insulators in solid and liquid state (In liquid state, Fermi surface energy may be chemical potential.), regardless of their dimensions, one, two or three.

Let us examine the similarity and difference between *Yuheng Zhang effect* and piezoelectric effect. Their similarity is that both of them happen due to strains caused by applied stress and they can generate separation of accumulated charges in some semiconductors and insulators [24]. However, their difference is obvious. First, rigorously speaking, *Yuheng Zhang effect* is induced by strain gradient in materials rather than uniform strains for piezoelectric effect; second, *Yuheng Zhang effect* might be valid for all condensed materials including crystalline materials with center-inversion symmetry, but piezoelectric effect only exist in insulating materials without center-inversion symmetry; third, *Yuheng Zhang effect* may applies for metals, however, piezoelectric effect does not.

The strain-induced electric potential is also compared with Galvani potential here. In some respect, this potential is like Galvani potential. Galvani potential occurs when two different materials contact each other, and it is given by difference between Fermi surface energies of the two materials [25], $qV = E_{F2} - E_{F1}$, where q is electron charge, V is the Galvani potential, E_{F1} and E_{F2} are the Fermi surface energy of the two different materials, respectively. If the material under different strains are regarded as different materials, this potential is the same as Galvani potential. But they differ from each other. This potential arises from strain-induced lift of Fermi surface energy of the identical material, whereas Galvani potential comes from the heterogeneous junction of two distinct materials with different Fermi surface energies.

Generally speaking, many methods could alter Fermi surface energy. As usually encountered in semiconductors, doping can change Fermi surface energy, e.g., donor doping and acceptor doping in silicon. Besides, temperature variations and magnetic field also enable Fermi surface energy lift, despite very small alteration in many materials. These related physical processes are interesting and might be described by *Yuheng Zhang equation*, but in this work the strain effects are mainly focused on.

Like in metals [23], this effect in semiconductors and insulators may also lead to several interesting phenomena.

3.1. P-n junction Behaviors

Non-uniformly strained materials, especially metal and narrow band semiconductors, may behave as a p-n junction, displaying current-rectifying behaviors and similar current-voltage (I-V) characters because of strain-induced electric potential as shown in Figure 2. And the biased electrical voltage V_Z equals to the Fermi surface energy difference. As for the strained materials and conventional p-n junction, actually, they are the same as each other in principle, because both of them are generated by altered Fermi surface energy. One is strain altering Fermi surface energy; the other is atom-doping altering Fermi surface energy, thereby both causing an electric voltage. This property may be crucial in some situations. For example, one must be careful when performing resistance measurement of materials experiencing non-uniform strain. As shown in Figure 2(b) (black line), the measured resistance might be larger than the actual values.

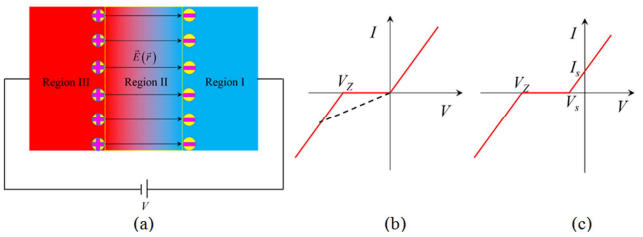

Figure 2. *Sketch of some metals and narrow band semiconductors under strain gradient as well as their current-rectifying properties. An assumption is taken that the strained regions possess higher Fermi surface energy. (a) stained materials in electrical circuit with an applied external electrical voltage V; Region I and Region III stand for the unstrained regions and strained regions, and Region II is strain gradient regions; stuffed circles with negative and positive signs present electrons and ions, respectively; arrows in Region II give the possible electric field distribution; (b) current-voltage (I-V) relation displayed by the metal and semiconductors under strain gradient, V_Z is strain-induced electric potential between Region I and Region III; (c) current-voltage (I-V) relation displayed by semiconductors under strain gradient, V_Z is strain-induced electric potential in equilibrium state and V_S presents the measured electric potential in non-equilibrium state.*

Another interesting point is that if the non-uniformly strained metals and semiconductors do not reach electric equilibrium state, a net current I_S and a net electrical potential V_S can be measured in an outer electrical circuit and related I-V characteristic line is shown in Figure 2(c). As shown, analogous to thermoelectric potential and Seebeck coefficient, a new coefficient S_{ij} could be introduced to describe this property.

$$\Delta V_m = -S_{ij}\Delta\epsilon_{ij} \tag{3}$$

where ΔV_m is the measured electric potential difference and $\Delta\epsilon_{ij}$ is strain component difference, the index obeys Einstein notation. It also could be written in another form

$$\vec{E}_m = S_{ij}\nabla\epsilon_{ij} \tag{4}$$

where E_m is measurable electric field $\vec{E}_m = -\nabla V$. This electric field could be obtained by electron electrochemical potential gradient

$$\nabla\mu = q\vec{E}_m \tag{5}$$

where μ is position dependence of electron electrochemical potential, and if the system reach their equilibrium state, it is a constant and the related electric field is zero. Thus, the coefficient S_{ij} is obtained

$$S_{ij} = \frac{\partial\mu}{q\partial\epsilon_{ij}} \tag{6}$$

Upon applying an external electrical voltage, the yielded heat is easily obtained

$$\dot{Q} = \sigma E_e^2 + \sigma E_e S_{ij}\nabla\epsilon_{ij} \tag{7}$$

where $\dot{Q}$ is generated power per unit volume in this material, E_e presents externally applied electric field, σ stands for electrical conductivity. Seen from this equation, if the applied external electric field E_e is in the same direction with the internal measurable electric field E_m, this material would release more heat. Otherwise it would release less heat. The interesting point is that if the external electric field E_e was opposite to and smaller than the electric field E_m, the material would absorb heat. These properties resemble the well-known Thomson effect that when an externa electrical current pass through a material with homogenous temperature gradient the material will release or absorb more heat [26]. The distinction is that here these properties are achieved in materials with strain gradient but Thomson effect is accomplished in materials with temperature gradient.

3.2. A New Solar Cell

Semiconductors with strain gradient can be utilized as a solar cell. Based on *Yuheng Zhang equation*, an electric field is generated in the strain gradient region, and thus the high Fermi surface region behaves as a n-doped zone and low Fermi surface region acts as a p-doped zone. Under sunlight radiation, electrons can be excited from valence band to conduction band, yielding conduction electrons and conduction holes. The yielded conduction electrons and holes will move to high Fermi surface region and low Fermi surface region respectively under action of this electric field, as is shown in Figure 3(a), resulting in an electrical voltage and electrical current in the outer closed electrical circuit. The theory describing electrical characteristics of new solar cell may be the same as that for the classical solar cell formed by p-n junction. At uniform temperature, if the parasitic resistances are not take into account, the current and the open circuit voltage may be given [27, 28].

$$I = I_{ph} - I_0\left(e^{qV/k_BT} - 1\right) \tag{8}$$

$$V_{OC} = \frac{k_BT}{q}\ln\left(\frac{I_{ph}}{I_0} + 1\right) \tag{9}$$

where q is electron charge, V_{OC} is yielded open circuit potential, I_{ph} presents photocurrent, the second term in Equation (8) is dark current, V is externally applied electrical voltage, k_B is Boltzmann constant, T is temperature, I_0 is reverse saturation current.

Let us perform the comparison between this new solar cell and conventional solar cell such as the widely applied silicon solar cells. Strictly speaking, they are the same as each other from viewpoint of basic physical principles. They both employ an internal electric field which arises from Fermi surface energy difference of semiconductors, and the electric field driving directional drift of conduction electrons and holes excited by photons will give birth to an electrical current and voltage. The only distinction lies in the fact that Fermi surface energy difference of conventional solar cells result from the doing, i.e., n-doping and p-doping, whereas for this new solar cell it comes from strain difference.

Upon clarifying physical principle of this new type of solar

cell, the remnant problem is how we can fabricate such a solar cell. A possible design may be shown in Figure 3(b). The lattice mismatch between the substrate and a single crystalline semiconductor thin film grown on it can produce a noticeable elastic strain gradient along thickness, which is usually observed for the epitaxially grown thin films [29]. Based on *Yuheng Zhang equation*, the strain gradient may give rise to the needed internal electric field, i.e., the key for a solar cell.

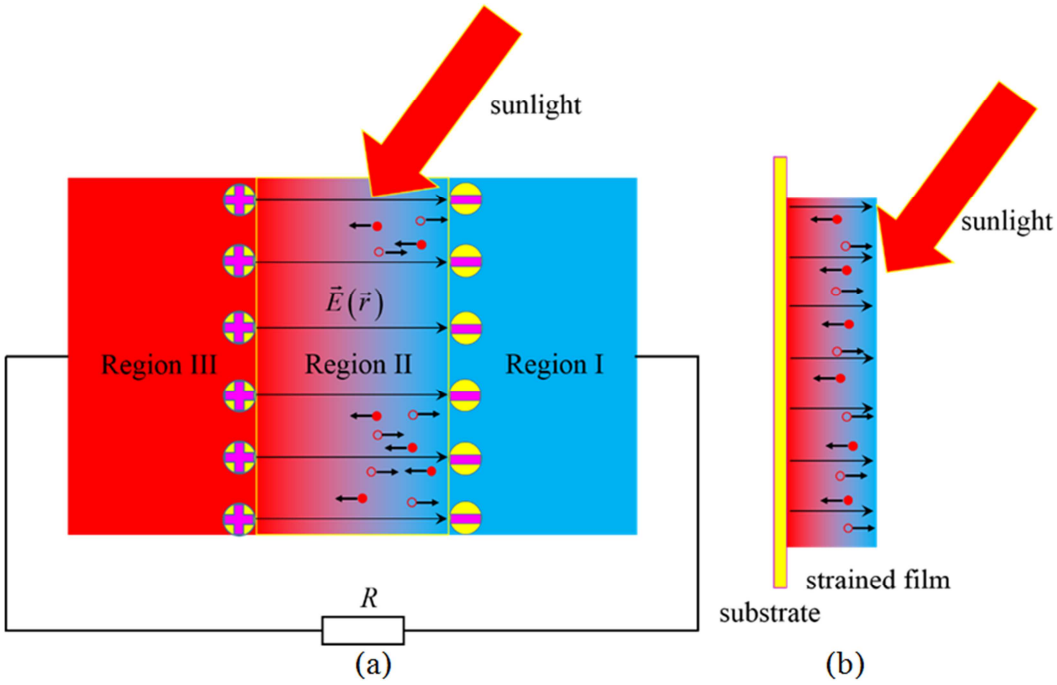

Figure 3. *Schematic diagram of a new type of solar cell. (a) a suitable semiconductor possessing strain gradient under sunlight: exited holes (denoted by red circles) move along the strain-induced electric field (presented by black arrows) and the related excited conduction electrons (denoted by red dots) move in the opposite direction, producing an electrical voltage across the region with strain gradient; (b) a possible design for such a solar cell under sunlight: a single crystalline thin film is grown on a substrate and a large strain gradient may be yielded due to lattice mismatch between the semiconductor and substrate, so that an electrical voltage may be offered.*

3.3. Thermoelectric Power

According to popular definition [30-33], theoretical Seebeck coefficient may be given by $S' = \vec{E}/\nabla T$, where $\vec{E}$ is electric field and ∇T is temperature gradient. According to *Yuheng Zhang effect*, thermal expansion may lead to an electric field $\nabla E_F/q$. The measured electric field originates from electrochemical potential difference [34] and it may be $\vec{E} - \nabla E_F/q$. So *Yuheng Zhang coefficient* [23] may be also valid,

$$S_Z = \frac{\alpha_V}{q}\frac{\delta E_F(\vec{r})}{\delta \ln V(T)} \tag{10}$$

where q is electron charge, $V(T)$ is temperature T dependence of volume and α_V is volume expansion parameter. Therefore, relation between experimental and theoretical Seebeck coefficient may be $S = S' - \partial E_F/q\partial T - S_Z$. Sometimes *Yuheng Zhang coefficient* may dominate temperature dependence of Seebeck coefficient, and its sign relies on both the thermal expansion parameter and strain dependence of Fermi surface energy. This may give a new understanding for temperature dependence of thermoelectric power of materials.

3.4. New source of Electron-phonon Interaction

Strains, including elastic and plastic strains, usually come from motion and redistribution of ions in materials. When ions move the electrons can quickly follow them and reach a new equilibrium state due to much smaller electron mass than ions. Consider a case that a longitudinal wave passing through a simple cubic crystal, due to induced periodic displacement of ions, a periodic strain may appear and therefore *Yuheng Zhang effect* occurs, generating an electric field and a related electrical potential, as is shown in Figure 4 (b) and (c). Electrons will experience the electric field and their potential energy is correspondingly lifted. This is the newly proposed mechanism of electron-phonon (*e-p*) interaction in this work. By means of similar calculations [35], its mathematic expression may be written as

$$H_{e-p} = -i\sum_{\vec{k},\vec{q},\lambda}\vec{\lambda}_q\cdot\vec{q}\sqrt{\frac{\hbar}{2MN\omega_{\vec{q},\lambda}}}E_F(\vec{q})\left(b_{\vec{q},\lambda}+b^+_{-\vec{q},\lambda}\right)C^+_{\vec{k}}C_{\vec{k}-\vec{q}} \tag{11}$$

where $H_{e\text{-}p}$ is *e-p* Hamiltonian, $b_{q,\lambda}$ and $b^+_{\vec{q},\lambda}$ are annihilation and creation operators for λ branch phonons with momentum q, $C_{\vec{k}}$ and $C^+_{\vec{k}}$ are annihilation and creation operators for electrons with momentum k, respectively, $\omega_{q,\lambda}$ is phonon

energy, M is ion mass, N is number of ions in the crystal, $\vec{\lambda}_q$ is a direction unit vector for ion vibrations, Fermi surface energy for electrons at ion position $\vec{R}_j$ is $E_F\left(\vec{r}-\vec{R}_j\right)$, and its Fourier form is $E_F\left(\vec{r}-\vec{R}_j\right)=\frac{1}{N}\sum_{\vec{k}}E_F\left(\vec{k}\right)e^{i\vec{k}\cdot\left(\vec{r}-\vec{R}_j\right)}$.

This new *e-p* interaction is very like the conventional *e-p* interaction [35] in formalism, but they are distinct in physics. This *e-p* interaction comes from *Yuheng Zhang effect*, but the conventional *e-p* interaction stems from screened coulomb interaction between ions and electrons. Strength of the new *e-p* interaction sensitively depends on functional derivative of $\delta E_F/\delta C$ (C is position dependence of strain, negative for compressed strain and positive for tensile strain) and can be more easily determined by first-principle calculations. Like the conventional *e-p* interaction, the new *e-p* interaction may play a vital role in understanding multi-physical properties of crystals.

At the end of this part, let us give a predicted interesting phenomenon. Suppose a crystal is periodically strained along a direction and we measure its resistance along this direction, as is shown in Figure 4(b). According to previous discussions, the measured electrical current may be

$$I_m=\frac{1}{R_0}\left(U_e-\frac{LV_Z}{L_0}\right) \tag{12}$$

where I_m is measured electrical current flowing through the crystal, R_0 is actual resistance, U_e is applied external electrical voltage, L is length of the crystal, L_0 is periodic strain length, V_Z is the induced electric potential in a period as shown in Figure 4(c) (d). It is typical electrical characters of charge density wave [36]. It can be seen that the measured resistance is always larger than its actual value. A shorter period and larger strain will cause a more notable increase of measured resistance. On the contrary, the measured resistance decreases if the external voltage increases. It may be the underlying physical mechanism of electrical behaviors of charge density wave.

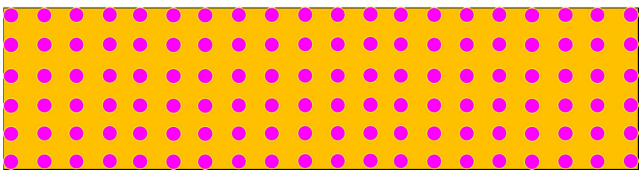

(a)

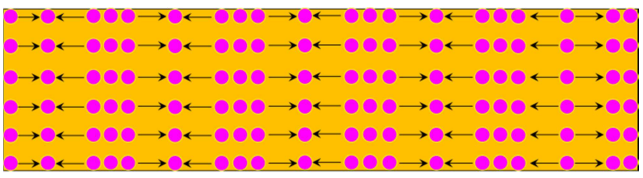

(b)

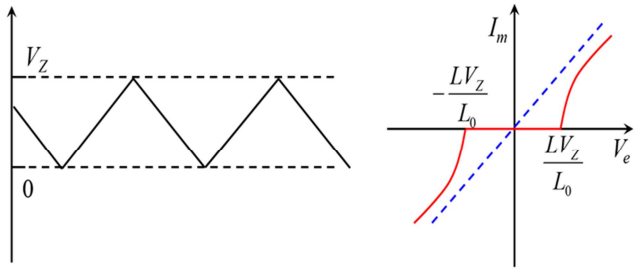

(c) (d)

Figure 4. *Schematic diagrams. (a) unstrained simple cubic (SC) crystalline lattice, the stuffed circles stand for ions; (b) periodically strained SC crystalline lattice, black arrows denotes the possible electric field distribution caused by Yuheng Zhang effect; (c) corresponding periodically electric potential for periodically strained crystalline lattice (b), where V_Z is the largest Yuheng Zhang potential in a period; (d) expected measured electrical current-voltage (I_m-V_e) relation and asymptotic line (blue dash line), where L is the crystal length, L_0 is wavelength of the longitudinal wave.*

3.5. Defects in Materials

3.5.1. Dislocations

In this part, we focus on electric properties of dislocations in terms of *Yuheng Zhang equation*.

Let us consider edge and screw dislocations in an isotropic material. According to elastic stress field of an edge dislocation [37] and Hooke's law, position dependence of local volume under the stress field of the dislocation is $V\left(x,y\right)=V_0\left[1-\frac{\left(1-2\nu\right)b_e}{2\pi\left(1-\nu\right)}\frac{y}{x^2+y^2}\right]$, where ν is Poisson's ratio, $V(x, y)$ is position (x, y) dependence of volume, V_0 is unstrained volume, b_e is Burgers vector of an edge dislocation in x direction. Ignoring boundary effect, e.g., image dislocation induced strain relaxation, based on Equation (1) and (2), the caused electric field around a single edge dislocation and electrical potential between any two points are easily obtained

$$\vec{E}\left(x,y\right)\approx\frac{V_0}{q}\frac{\delta E_F}{\delta V}\frac{\left(1-2\nu\right)b_e}{2\pi\left(1-\nu\right)}\left[\frac{2xy}{\left(x^2+y^2\right)^2}\vec{x}+\frac{y^2-x^2}{\left(x^2+y^2\right)^2}\vec{y}\right] \tag{13}$$

$$V_Z\left(x_2,y_2\right)-V_Z\left(x_1,y_1\right)\approx\frac{V_0}{q}\frac{\delta E_F}{\delta V}\frac{\left(1-2\nu\right)b_e}{2\pi\left(1-\nu\right)}\left(\frac{y_2}{x_2^2+y_2^2}-\frac{y_1}{x_1^2+y_1^2}\right) \tag{14}$$

where q is electron charge, $\vec{x}$ and $\vec{y}$ are unit direction vectors in cartesian coordinates. The electric field is shown in Figure 5(b). Another electric component $\delta E_F/\delta C_{12}\nabla C_{12}$ (C_{12} is shear strain) resulting from shear strain may be much smaller than main components in Equation (13) for an isotropic material and is neglected here, nevertheless, for other materials this component must be considered. By means of simple estimations, the electric field near the core of edge dislocation may approach a value as high as 10^8 V/m. Note that the electric field and potential strongly rest with $V_0\,\delta E_F/\delta V$, an intrinsic feature of a material. For sodium chloride, if $V_0\,\delta E_F/\delta V$ is positive, the dislocation may behave as an entirety of positive charges in tensile regions and negative

charges in compressed regions, and their charge densities are highest at the core as is shown in Figure 5(a). For instance, for a NaCl bar plastically bent under tensile load, a tensile strain field may be generated at convex surface and a compressed strain field may be yielded at concave surface, respectively, thereby creating positive charges at the convex surface and negative charges at the concave surfaces, which is indeed the experimental observations [18].

Another type of widespread dislocations, screw dislocations, only induce shear strains in an isotropic material [37]. Using Equation (1) in the same way, the induced electric field, potential difference and electric energy around a screw dislocation may be obtained as followings,

$$\vec{E}(x,y)=\frac{1}{q}\frac{\delta E_F}{\delta \epsilon_{13}}\frac{b_s}{2\pi}\left[\frac{-x^2+y^2+2xy}{\left(x^2+y^2\right)^2}\vec{x}+\frac{-x^2+y^2-2xy}{\left(x^2+y^2\right)^2}\vec{y}\right] \quad (15)$$

$$V_Z(x_2,y_2)-V_Z(x_1,y_1)\approx-\frac{1}{q}\frac{\delta E_F}{\delta \epsilon_{13}}\frac{b_s}{2\pi}\left(\frac{x_2-y_2}{x_2^2+y_2^2}-\frac{x_1-y_1}{x_1^2+y_1^2}\right) \quad (16)$$

where b_s is Burgers vector of this screw dislocation in z direction, ϵ_{13} is induced shear strain by this screw dislocation. In isotropic materials, this relation may exist $\left|\delta E_F/\delta \epsilon_{13}\right|<<\left|\delta E_F/\delta \epsilon_{11}\right|$ and there is no electric charges at its core. Therefore, *Yuheng Zhang effect* and its electric field around a screw dislocation may be not as apparent as that of edge dislocations, as is the point observed by experiments [18].

The electric field around dislocations necessarily brings electric energy. For an isotropic linear dielectric material, the electric energy for a dislocation of unit length may be easily obtained in terms of Equation (13) and (15),

$$G_e\approx\frac{\varepsilon_0\varepsilon}{4\pi}\left(\frac{V_0}{q}\frac{\delta E_F}{\delta V}\right)^2\frac{(1-2\nu)^2 b_e^2}{(1-\nu)^2 r_{e0}^2} \quad (17)$$

$$G_s\approx\frac{\varepsilon_0\varepsilon}{4\pi}\left(\frac{1}{q}\frac{\delta E_F}{\delta \epsilon_{13}}\right)^2\frac{b_s^2}{r_{s0}^2} \quad (18)$$

where ε is relative dielectric permittivity, G_e, G_s is electric energy surrounding an edge dislocation and a screw dislocation, respectively, r_{e0}, r_{s0} is radius of the corresponding edge dislocation core and screw dislocation core. For some dielectric materials, this energy may be comparable with or even larger than the elastic energy of dislocations.

In the case of metals, the calculation of electric energy may be a little complicated due to the difficult selection of relative permittivity. A potential candidate may reside in Thomas-Fermi screening dielectric function, i.e., the static limit of Lindhard dielectric function. Take the same approximation as in calculations of the earth's geomagnetic field [38] and it is

$$\varepsilon_0\left(e^{r/r_s}-1\right)E=n_e q r\approx C \quad (19)$$

where r_s is Thomas-Fermi screening length, n_e denotes free electron density in metals, q stands for electron charge and E is electric field strength. For dislocation inducing static electric field in most of metals, C may approximate ~−10 C/m^2. Thus, electric energies around an edge dislocation and a screw dislocation is obtained,

$$G_e\approx\left|\frac{C}{q}\frac{V_0\delta E_F}{\delta V}\frac{(1-2\nu)b_e}{(1-\nu)}\right|\ln\frac{R}{r_{e0}} \quad (20)$$

$$G_s\approx\left|\frac{\sqrt{2}b_s C}{q}\frac{\delta E_F}{\delta \epsilon_{13}}\right|\ln\frac{R}{r_{s0}} \quad (21)$$

where R is radius of strained regions. The calculation only give rough estimation of electric energies of dislocations in metals, and more accurate calculations still need to be explored.

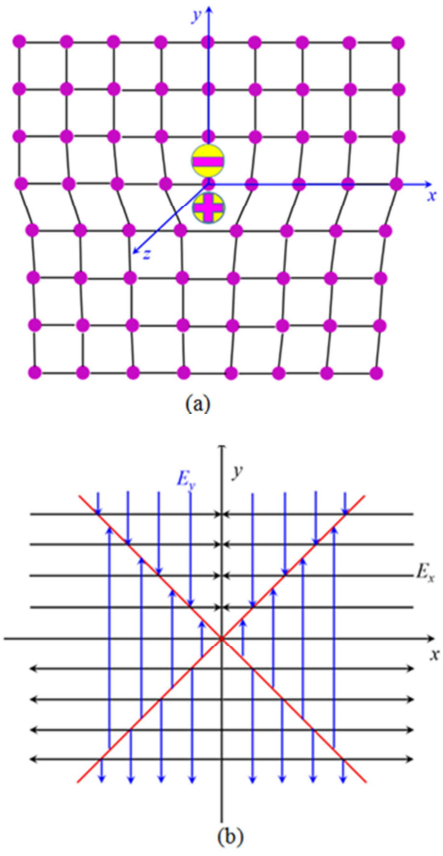

Figure 5. *Sketch of an edge dislocation (a) and its electric field distribution (b) in an isotropic material. (a) stuffed purple circles denote atoms or ions, short black line are bonds, positive and negative stuffed yellow circles are line positive and negative charges, respectively; (b) black and blue arrows present direction of electric field E_x and E_y, but do not denote strength of these fields.*

According to above discussions, total energy of a dislocation may consist of two parts, one is the well-known elastic energy, the other is the electric energy which may be pointed out for the first time here. When analyzing dislocation dominated mechanical properties of materials, one must take this electric energy into account. Due to electrostriction effect,

the electric field reversely leads to strains which may modify strain field of dislocations. In the other respect, the dislocations may affect electrical resistance of materials. In view of the electric fields of edge and screw dislocations (Figure 5(b)), electrical resistance in *x*-*y* plane may increase conspicuously as is usually observed in metals and semiconductors [39-41], but electrical resistance along *z* direction may not be influenced due to absence of *z*-component electric field. This mechanism provides people a simple route to understand dislocation effect on electrical resistance. For isotropic materials, main strain-induced lift of E_F may be much larger than that caused by shear strain, therefore, the edge dislocations may dominate variations of electrical resistance. For anisotropic materials, one must consider influence of both the two types of dislocations on electrical resistance.

Moreover, electric effects of dislocations and other strained mechanical microstructures may also be important in related chemical areas, e.g. electrochemical corrosion.

3.5.2. Other Point Defects

Analogous to the case of dislocations, beside elastic stress field around them, other point defects such as interstitial atoms, vacancies, impurity atoms and so on usually give rise to radial strain field around them. In light of *Yuheng Zhang equation*, the radial strain may generate radial electric field. Using Gauss's law, one may find that the point defects act as charged particles in materials and increase electrical resistance in all crystalline orientations. When analyzing multi-physical properties of materials, one must consider both elastic field and related radial electric field.

3.5.3. Abrikosov Vortex

In type-II superconductors, when the external magnetic field is higher than critical field H_{C1}, magnetic field will enter the superconductor and forms some vortices. For an isolated vortex, density of Cooper pairs is suppressed to zero at its center and restores its full value at a distance of coherence length ξ away from the center [42]. Within the vortex, materials stay in magnetic field and its magnetic pressure coming from Lorenz force may be $P(r)=B^2(r)/2\mu_0$ [43], where $P(r)$ is magnetic pressure, r is distance from the center of vortex, $\mu_0=4\pi\times10^{-7}$ *H*/*m* is vacuum magnetic susceptibility. At the center of vortex, superconducting state is believed to be completely destroyed, and the corresponding magnetic field might reach upper critical field, *i.e.*, $B(0)=B_{C2}(T)$. So, the generated tensile magnetic pressure at the center is

$$P(0)=\frac{B_{C2}^2(T)}{2\mu_0} \tag{22}$$

For type-II superconductors, the upper critical field varies as temperature and is usually of order ~10 *T* at low temperatures [44-46]. The generated tensile magnetic pressure may be $P(0)\approx40$ *MPa*, comparable with yield strength of many metals, and the induced volume strain may reach ~10^{-4}. Based on *Yuheng Zhang equation*, if magnitude $\delta E_F/\delta C$ ranges from 1 to 10 *eV*, the produced potential $V_Z(T)$ will be in the range 0.1~1 *mV*. On the other hand, strong magnetic field may also alter the Fermi surface energy of this normal region a little by $\mu_B \cdot B_{C2}(T)$~0.6 *meV*, producing another potential. So, the whole electrical potential between center of vortex and its surrounding areas may be summation of the two potentials. Like temperature dependence of upper critical field $B_{C2}(T)$, the potential is strongly temperature dependent and decreases rapidly as temperature increases. Conversely, measurement of temperature dependence of electrical potential $V_Z(T)$ for a single vortex may offer people another method to determine temperature dependence of upper critical field $B_{C2}(T)$, particularly upper critical field of some high-temperature superconductors such as cuprate superconductors and iron-based superconductors. Owing to the electric properties, Abrikosov vortices are expected to behave as line charges sometimes.

3.5.4. Magnetic Domain Walls and Magnetic Skyrmions

When a ferromagnetic (FM) material is subject to external magnetic field, Fermi surface energy of magnetic domains parallel to magnetic field may be lower than that of domains antiparallel to the magnetic field. In case of popular 180° domain walls, Fermi surface energy may be lifted by $2S\mu_B B$ across the domain wall, where $S\mu_B$ is magnetic moment at a site, μ_B is Bohr magneton, B is external magnetic field. So according to *Yuheng Zhang equation*, an electric field and an electrical potential may appear within the domain wall. Assume 1 *T* of the external magnetic field, $2\mu_B$ of the magnetic moment, and 30 *nm* of the domain wall thickness, the corresponding electrical potential and related electric field may approach ~0.2 *mV* and ~7×10^3 *V*/*m*, respectively.

Like the case of magnetic domain walls, a recent hot and interesting topic of a topological defect, magnetic skyrmion, may display similar electric properties under external field and may yield an electrical potential and a radial electric field between center of skyrmion and its surroundings. In a sense, skyrmions also behave as charged quasiparticles under external magnetic field, which means that it could be tuned by an external electric field.

3.6. Phase Transition Induced Electrical Voltage at Interface

As discussed for metals [23], when phase transition happens for a material, Fermi surface energy of the new phase may be lifted due to volume and symmetry changes. So, an electrical voltage and electric polarization may appear at the interface between the material and its new phase in spite of their identical chemical compositions. This voltage may be written as $qV_{12}=E_{F2}-E_{F1}$, where V_{12} is voltage at the interface, q is electron charge, E_{F1} and E_{F2} are the Fermi surface energy of the material and its new phase, respectively. This voltage may be unique and likes a fingerprint, and can be utilized to characterize phase transitions, especially the liquid-liquid transitions which are challenging for ordinary diagnostic methods.

3.7. Strain Induced Electric Field and Polarization

3.7.1. Strain Gradient Induced Electric Polarization

Upon strain gradient, insulators may present an electric polarization and it is obtained by means of *Yuheng Zhang equation*,

$$\vec{P}(\vec{r}) = \varepsilon_0(\varepsilon - 1)\frac{\nabla E_F(\vec{r})}{q} \tag{23}$$

where $\vec{P}(\vec{r})$ is position dependence of electric polarization, ε_0 and ε are vacuum dielectric permittivity and relative permittivity, respectively. Obviously, for a given material, the electric polarization depends on gradient of Fermi surface energy, and a larger position gradient of Fermi surface energy would lead to a larger electric polarization. For instance, the electric polarization may be very large within rarefaction waves and shock wave front which will be discussed later.

3.7.2. Mechanical Fracture of Material

For cases of mechanical loading exceeding fracture strength of a solid material, a fracture appears and a crack propagates in the material and stress concentration usually occurs at the tip of crack, especially for some ductile metals. The crack propagation is usually accompanied by elastic strain energy release and strain release at its two lateral sides, including initial concentrated crack tip stress and strain. The dynamic mechanical processes may give rise to *Yuheng Zhang effect*, thereby creating an electric field and electrical potential along unloading directions. From the viewpoint of energy, when a crack starts and propagates, the elastic strain energy transforms to fracture energy and electric energy, despite much smaller value of the electric energy than fracture energy sometimes. So the strain induced polarization state may help people examine strain state of a material under loading.

3.7.3. Gravity Induced Electric Field in Planets

Some materials naturally exhibit strain gradient due to gravity, *e.g*. various types of rocks in some planets and satellites in the aerospace. Generally speaking, a rock stays in planets deeper, it is subject to a larger pressure and thereby displays a larger compressed strain, resulting in a radial electric field and a corresponding electric polarization. The field strength may reach an order of $\sim 10^{-6}$ *V*/*m*. However, the actual electric field may be relatively complicated because of many different types of rocks and minerals as well as their complex distributions in planets and satellites.

Information of electric field distributions of minerals in the earth may be employed to unravel evolution of their stress and strain state. Of specially pointed out is the possibility that in terms of scanning internal electric field of minerals in the earth's crust, earthquake forecast, a highly desired but great challenge for people, might be viable in the future.

3.8. Microscopic Origin of Flexoelectric Effect

Flexoelectric effect was stated by phenomenological analysis more than half a century ago and it is believed that strain gradient has directionality and can yield an electric polarization in dielectric materials [47]. The flexoelectric polarization is given by the following relation [22],

$$P_l = \mu_{ijkl}\frac{\partial \epsilon_{ij}}{\partial x_k} \tag{24}$$

where P_l is the *l*-th component of flexoelectric polarization, μ_{ijkl} is flexoelectric coefficient and a fourth-rank polar tensor, ϵ_{ij} is position dependence of strain and x_k is position coordinate. Previous theoretical analysis [47, 48] estimated that magnitude of flexoelectric coefficient was very small and was the order of $q/a \sim 10^{-10}$ *C*/*m* (*q* is electron charge and *a* is lattice parameter), meaning that flexoelectric effect might be too small to tune polarization of materials. However, it was later found that flexoelectric coefficient can reach an unexpected large value and the related flexoelectric effect can dominate electric polarization of a material. For an instance, magnitude of flexoelectric coefficient is order of 10^{-6} *C*/*m* in relaxor ceramics $Pb(Mg_{1/3}Nb_{2/3})O_3$ [49], several orders higher than formerly estimated; and stress gradient can mechanically switch polarization in ferroelectric film [50]. Since then many progresses have been made in this area, including its phenomenological description [51], but the underlying microscopic physical origin is still a puzzle.

Here, it is stated and believed that flexoelectric effect is a special case of *Yuheng Zhang effect* in dielectric materials. And the microscopic origin may be provided by *Yuheng Zhang equation, i.e*., Equation (1). So, the induced electric polarization is given

$$P_l = \frac{\varepsilon_0(\varepsilon - 1)}{q}\frac{\delta E_F(\vec{r})}{\delta \epsilon_{ij}(\vec{r})}\frac{\partial x_k}{\partial x_l}\frac{\partial \epsilon_{ij}(\vec{r})}{\partial x_k} \tag{25}$$

where $\epsilon_{ij}(r)$ is position dependence of strain, *q* is electron charge. By comparing Equation (24) and (25), the flexoelectric coefficients can be obtained easily,

$$\mu_{ijkl} = \frac{\varepsilon_0(\varepsilon - 1)}{q}\frac{\delta E_F(\vec{r})}{\delta \epsilon_{ij}(\vec{r})}\delta_{kl} \tag{26}$$

where δ_{kl} is unity only when the subscript is the same as each other (δ_{kl}=1 for *k*=*l*; δ_{kl}=0 for others). So, the flexoelectric coefficients can be reduced and expressed as,

$$P_l = \mu_{ij}\frac{\partial \epsilon_{ij}(\vec{r})}{\partial x_l} \tag{27}$$

$$\mu_{ij} = \frac{\varepsilon_0(\varepsilon - 1)}{q}\frac{\delta E_F(\vec{r})}{\delta \epsilon_{ij}(\vec{r})} \tag{28}$$

According to Equation (28), flexoelectric coefficients are monitored by two key parameters: one is the relative permittivity ε, the other is strain dependence of Fermi surface energy $\delta E_F(\vec{r})/\delta\epsilon_{ij}(\vec{r})$. For most of materials, $\left|\delta E_F(\vec{r})/\delta\epsilon_{ii}(\vec{r})\right|$ may be in the range 1~10 *eV*, thus the magnitude of corresponding flexoelectric coefficients are summarized in Table 1. In the case of relaxor $Pb(Mg_{1/3}Nb_{2/3})O_3$ whose relative permittivity is 13000 at 1 *KHz* and room temperature, flexoelectric experimental measurement gives the corresponding flexoelectric coefficient 4×10^{-6} *C/m* [49], which is in qualitative agreement with estimation in Table 1. For epitaxial single crystalline $BaTiO_3$ thin film under compression, based on its calculated volume variations [50], the electric field estimated by *Yuheng Zhang equation* gives $5\times10^7\sim5\times10^8$ *V/m*, which is in accord with the measured biased field ~10^8 *V/m* in the hysteresis loop in supplementary materials [50]. Further quantitative work may need to carry out first-principle calculations to determine the parameter $\delta E_F(\vec{r})/\delta\epsilon_{ij}(\vec{r})$ of these materials.

Table 1. *For most materials with possible volume dependence of Fermi surface energy $\left|\delta E_F(\vec{r})/\partial\epsilon_{ii}(\vec{r})\right|$ in the range 1~10 eV, the obtained flexoelectric coefficients are listed as followings.*

Relative permittivity ε	**Flexoelectric coefficients $\mu_{ii}=\left\|\frac{\varepsilon_0(\varepsilon-1)}{q}\frac{\delta E_F(\vec{r})}{\delta\epsilon_{ii}(\vec{r})}\right\|$**
1-10	$10^{-11}\sim10^{-9}$ *C/m*
10-100	$10^{-10}\sim10^{-8}$ *C/m*
100-1000	$10^{-9}\sim10^{-7}$ *C/m*
1000-10000	$10^{-8}\sim10^{-6}$ *C/m*

3.9. Strain Engineering

In thin films epitaxially grown on substrate, strains usually stem from lattice mismatch between the film material and substrate. For the mismatch-induced strains, there exist a critical thickness within which the strains offer an opportunity to enhance some physical properties of the film and beyond which the strains are not available [29]. The out-of-plane strain can be expressed by the following form [29],

$$\epsilon(r)=\epsilon_0 e^{-r/d_c} \tag{29}$$

where $\epsilon(r)$ stands for out-of-plain strain in the film at a distance r away from the interface, d_c is the related critical thickness, and ϵ_0 is the out-of-plain strain at the interface. The critical thickness is usually tens of nanometers, and strain gradient in oxide epitaxial thin films such as $HoMnO_3$ can often approach a value as large as 10^6 */m* [52]. Combining *Yuheng Zhang equation* and Equation (29), one may easily find that the generated internal electric field is usually perpendicular to the interface. For the self-polarized ferroelectric domain, i.e., upward or downward polarization shown in thin films in their as-grown state [52], it may be the physical origin.

To ascertain whether the proposed point is right or not, the corresponding comparison is performed between the theory and experiments. In terms of *Yuheng Zhang equation*, if the corresponding parameter $\delta E_F(\vec{r})/\delta\epsilon_{ii}(\vec{r})$ for $HoMnO_3$ is order of ~10 *eV*, the yielded intrinsic electric field might be 10^7 *V/m* agreeing with experimental biased electric field ~4×10^7 *V/m* measured in the hysteresis loop for the ferroelectric monodomain [53]. Investigations on strained $SrTiO_3$ epitaxial thin film suggest that the mismatch strain play a similar role as an electric field in polarization [54]. For simplicity, as an estimation, the strain gradient could be taken as ratio between strain and film thickness 2×10^5 */m* and therefore the induced electric field may achieve 10^6 *V/m*, a value consistent with the biased field ~2×10^6 *V/m* in measured hysteresis loop [54]. In a word, these experiments may verify correctness of *Yuheng Zhang equation* and *Yuheng Zhang effect*, albeit qualitative nowadays.

3.10. Microscopic Theory of Shock Polarization

For shock-loaded materials as shown in Figure 1, strain-induced electrical potential and its corresponding electric polarization always exist across the shock wave front (region II in Figure 1) no matter how weak the shock wave is and no matter whether plasticity occurs or not. Based on *Yuheng Zhang equation*, magnitude of this potential and electric polarization relies on shock waves. A stronger shock wave may lead to a larger electrical potential and a larger electric polarization.

In this work, it is proposed and stated that shock polarization is another representation of *Yuheng Zhang effect* in materials under shock loading. The corresponding microscopic mechanism may be given by *Yuheng Zhang equation*.

Figure 6 (a) gives the typical experimental setup for the measurements [4, 9, 55], and its equivalent electrical circuit is shown in Figure 6 (b) and (c). On imparting a screening metal plate (Electrode I) by a flyer plate, shock waves emerge and compress the metal electrode, thereby creating an electrical potential V_{S1} in this electrode (left brown zones in Electrode I). Before shock wave reaching interface between Electrode I and the investigated materials, its equivalent electrical circuit is given by Figure 6 (b). As a result, there is no electrical signals, which is consistent with experimental results [4, 9, 55].

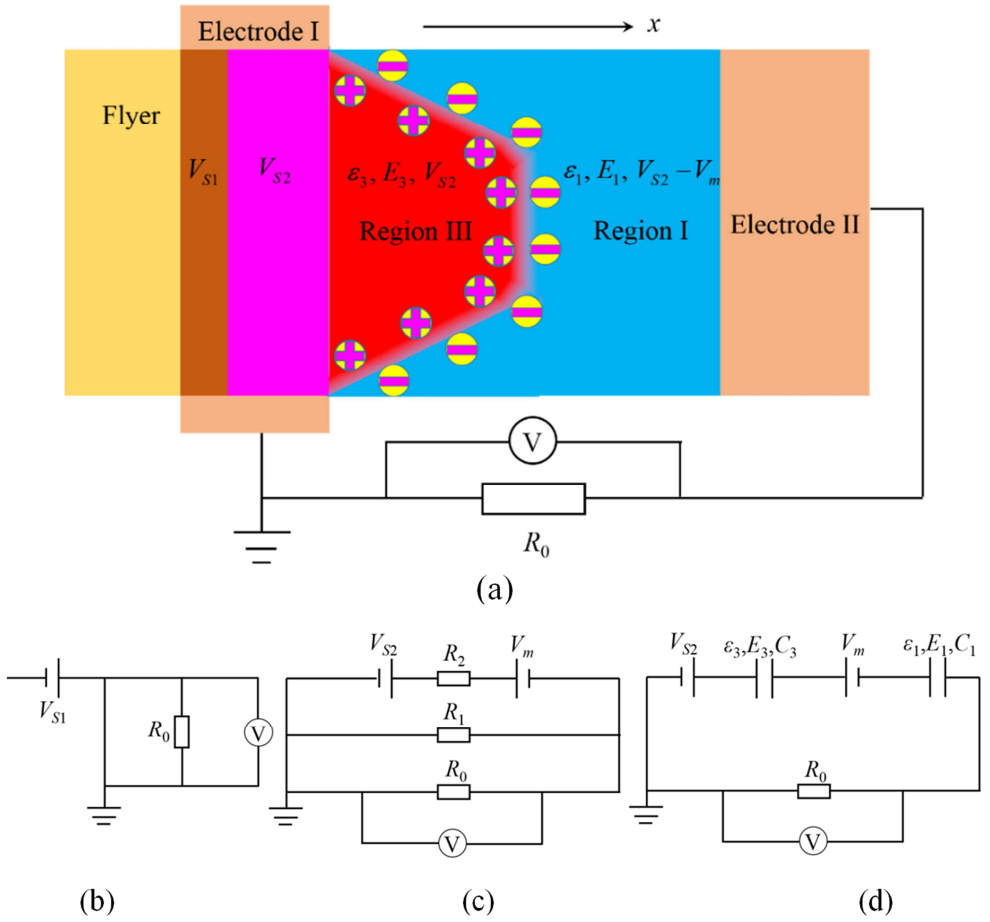

Figure 6. *Schematic diagram of experimental setup (a) and corresponding equivalent electrical circuits (b), (c) and (d). In experimental setup (a), a flyer plate (left yellow zone) impacts an electrical screening plate which is also used as electrode I (left orange zones) and creates shock waves (left brown zone) which generate a Yuheng Zhang potential V_{S1} in electrode I, and (b) is the related electrical circuit. When arriving at interface between the screening plate and investigated material, the shock waves penetrate into the investigated material (light blue zones) and compress it (red zones). Across shock wave front (color gradient zone) in the material, another potential appears and is denoted as V_m. Electrode II, the same metal material as electrode I, is adopted and is connected to an external resistance R_0. Its voltage is the measured voltage. If the investigated material is a metal, its equivalent electrical circuit is shown in (c), while electrical circuit for a dielectric material is shown in (d). The relative permittivity, electric field, capacitance, resistance for the dielectric material in shocked regions (red zones) and un-shocked regions (light blue zones) are ε_3, E_3, C_3 and ε_1, E_1, C_1, respectively.*

3.10.1. Electromotive Force (EMF) in Shocked Metals

When shock waves arrive at the boundary between Electrode I and investigated metal, they enter the metal and compress it (red zones), generating a potential V_m between shocked regions and un-shocked regions as shown in Figure 6(a). Simultaneously another wave is reflected into Electrode I, compressing or decompressing Electrode I further (If shock impedance of investigated material is larger than that of Electrode I, the reflected wave is a shock wave that compresses Electrode I, otherwise it is rarefaction waves decompressing the electrode.). Therefore, another potential V_{S2} is yielded in Electrode I (magenta zones) as shown in Figure 6(a). The equivalent electrical circuit is given by Figure 6(c). If the investigated metal is the same as electrode metal, no wave is reflected from the interface, and the potentials V_{S2}, V_m in circuit (Figure 6(c)) equals to the potential V_{S1}, *i.e.*, V_{S2}= V_m=V_{S1}. Therefore, there is no electrical signals, which is in agreement with experimental results [56].

Now let us focus on the case that the electrodes and investigated sample are different metals. All the formed plane boundaries between electrodes and sample could be regarded as good electrical contacts in the circuit shown in Figure 6(c). In the circuit, a resistance R_2 denotes intrinsic resistance of metal sample, electrodes and their contact resistance. A resistance R_1 stands for contact resistance between electrode I and released lateral regions in the metal sample (light blue regions in Figure 6(a)), the contact area may be a very narrow ring. The two resistances may be much smaller than the external resistance R_0 which is in the range 50~100 Ω in the measurements [4, 9, 54, 57]. So the measured voltage might be

$$V_0 = \frac{R_1 (V_{S2} - V_m)}{R_1 + R_2} \tag{30}$$

$$qV_{S2} = E_{FS}(\epsilon_{S2}) - E_{FS}(0) \tag{31}$$

$$qV_m = E_{Fm}(\epsilon_m) - E_{Fm}(0) \tag{32}$$

where V_0 is the measured voltage, V_{S2}, V_m and E_{FS}, E_{Fm} are

electrical potential and Fermi surface energy of screening metal plate and sample, respectively, C_{S2}, C_m is related strains of screening metal plate and sample (negative for compressed strain and positive for tensile strain).

Due to uncertainty in the experiments, the accurate values of the two resistances is difficult to determine, which may be the reason for conspicuous discrepancy of the measured voltage in different groups [4, 56, 58]. However, it can give the sign of the measured voltage. If the potentials fulfill $V_{S2}-V_m>0$, the measured voltage is positive, and conversely it is negative. If a metal possessing both high Fermi surface energy and low shock impedance is used as screening metal plate, in other words, a large positive potential V_{S2}, the measured voltage seems more to be positive, otherwise it is more possible to be negative, which agrees with experimental results [4]. Interestingly, according to Equation (30), if an insulating material whose shock impedance matches that of sample is placed around the sample, *i.e.*, increasing R_1 dramatically, the measured voltage would increase and be close to the value ($V_{S2}-V_m$). This point still needs experiments to prove in the future.

Of noted is that in the above analysis on EMF in metals, the thermoelectric power and phase transition are not considered. Both of them can contribute to the experimental results, especially the latter one. To be anticipated, when phase transition happens, it usually causes a sudden magnitude change or a sign change of the measured voltage. The precise value of phase-transition-induced electrical voltage still need much theoretical and experimental work to determine.

3.10.2. EMF in Shocked Semiconductors and Insulators-shock Polarization

As for most of semiconductors and insulators, their resistivity is usually larger than $10^6\ \Omega\cdot m$. So for a sample with a thickness ~mm and an area ~cm^2, its resistance is much larger than the external resistance R_0 in a range 50-100 Ω. If the resistance of sample in compressed regions does not decrease sharply and is still much larger than external resistance R_0, the related electrical circuit could be simplified as shown in Figure 6(d), which is analogous to a previous phenomenological explanation for shock polarization [7]. The shocked regions and unshocked regions of sample may act as two parallel-plate capacitors with relative permittivity ε_3, electric field E_3, capacitance C_3 and ε_1, E_1, C_1, respectively. The time dependence of measured electrical current and voltage are given as

$$I(t)=\frac{dC_3V_3}{dt} \tag{33}$$

$$I(t)=\frac{dC_1V_1}{dt} \tag{34}$$

$$I(t)R_0=V_{S2}-V_m-V_3-V_1 \tag{35}$$

where $I(t)$ is time dependence of electrical current passing the circuit (positive for clockwise), V_3 and V_1 are the voltages at the two capacitors, respectively. After some simple calculations, it is

$$\frac{dE_1(t')}{dt'}+\left[\left(\lambda_3-\lambda_1\right)t'+\lambda_1\right]E_1(t')=\lambda_1E_0 \tag{36}$$

where the parameters $\lambda_1=t_0/\tau_1$, $\lambda_3=t_0/\tau_3$, $\tau_1=A\varepsilon_0\varepsilon_1R_0/L$, $\tau_3=A\varepsilon_0\varepsilon_3R_0/(U-u)t_0$, $t'=t/t_0$, $V_1=U(t_0-t)E_1(t)$, $V_3=(U-u)tE_3(t)$, $L=Ut_0$, $E_0=(V_{S2}-V_m)/L$, U is shock wave velocity and u is the particle velocity, L is thickness of the sample, A is area of sample, t_0 is time duration for shock waves passing the sample, E_1 is electric field in capacitor C_1. Based on these equations, the measured time dependence of electrical current is

$$I(t')=\frac{V_{S2}-V_m}{R_0}\left\{1-\sqrt{\frac{\pi\lambda_3(k-1)}{2}}\left(\frac{k}{k-1}-t'\right)e^{\frac{\lambda_3(k-1)}{2}\left(t'-\frac{k}{k-1}\right)^2}\left[Erf\left(\sqrt{\frac{\lambda_3}{2}}\frac{k}{\sqrt{k-1}}\right)+Erf\left(\sqrt{\frac{\lambda_3(k-1)}{2}}\left(t'-\frac{k}{k-1}\right)\right)\right]\right\} \tag{37}$$

where parameter $k=\lambda_1/\lambda_3$, $Erf(x)$ is error function. Seen from this equation, the current versus time relation $I(t')$ only depends on parameters k and λ_3. To clarify roles of sample area, thickness and relative permittivity and so on, let sample area $A=A_u\times10^{-4}\ m^2$, external resistance $R_0=R_u\times50\ \Omega$, $V_{S2}-V_m=V_u\times1$ V, velocity $U-u=U_u\times10^3\ m/s$, permittivity $\varepsilon_0\varepsilon=\varepsilon_u\times10^{-11}\ F/m$ and duration $t_0=t_u\times10^{-6}\ s$, where A_u, R_u, U_u, ε_u and t_u are dimensionless parameters. Substitute them into Equation (37), it is

$$I(t')=\frac{0.02V_u}{R_u}\left\{1-10^2t_u\sqrt{\pi(k-1)}\sqrt{\frac{U_u}{A_u\varepsilon_uR_u}}\left(\frac{k}{k-1}-t'\right)e^{\frac{10^4U_ut_u^2}{A_u\varepsilon_uR_u}(k-1)\left(t'-\frac{k}{k-1}\right)^2}\left[Erf\left(10^2t_u\sqrt{\frac{U_u}{A_u\varepsilon_uR_u}}\frac{k}{\sqrt{k-1}}\right)+Erf\left(10^2t_u\sqrt{\frac{(k-1)U_u}{A_u\varepsilon_uR_u}}\left(t'-\frac{k}{k-1}\right)\right)\right]\right\}$$

According to this equation, the typical results, current-time relation $I(t')$-t' are shown in Figure 7. It shows that $I(t')$-t' line presents a down-concave shape (see Figure 6(a)), and interestingly, magnitude of the current relies on both sample areas and durations, in other words, sample thickness. The electrical current gradually increases with increasing sample area, and it remarkably rises as sample thickness declines (see Figure 7(b)), which are consistent with experimental results for single crystal sodium chloride NaCl [9, 55]. Through analysis, it is found that these properties arise from the pronounced increase of relative permittivity of materials in compressed regions. To one's surprise, if the relative permittivity decreases after shock compression, the current decreases as time and would display a sign change as shown in Figure 7(c), which may be reasons for the observed sign change for shock-loaded single crystal NaCl at 1 and 1.6 *GPa*

[9, 55]. In reality, the sign of current primarily depends upon variations of electrical potentials V_{S2} of the metal screening plate and V_m of the sample under compression. As discussed previously, the current is positive in the case of $V_{S2}-V_m>0$, but is negative in the opposite case. Furthermore, another $I(t')$- t' relation is predicted as shown in Figure 7 (d), which needs to be proved in the future. These primary results are stable in broad parameter zones. And the quantitative comparison with experiments nevertheless need first-principle calculations to determine potential values V_{S2} and V_m.

In terms of above discussions, shock polarization, a widespread phenomenon in materials under shock loading, may be fundamentally understood by using *Yuheng Zhang equation*. However, of emphasized is that phase transition, piezoelectric effect and self-polarization such as ferroelectric polarization and so on are not taken into account here. When one investigates a specific material under shock loading, he (she) must consider all possible factors.

According to previous discussion, a notable electric field may exist at the shock wave front and it may also be of paramount importance in some other fields, e.g. detonation initiation.

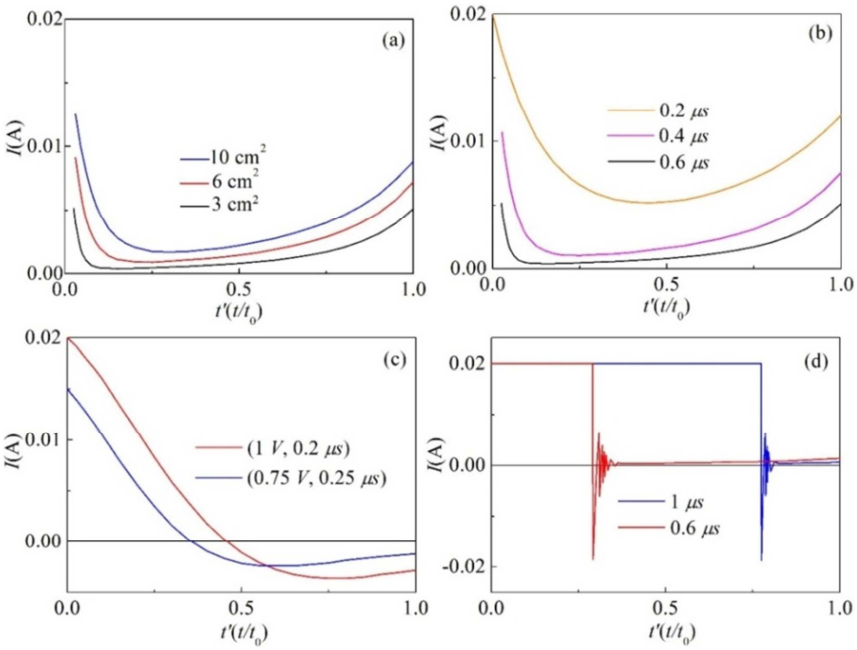

Figure 7. *Calculated results for current-time relation (I-t') for shock polarization. (a) sample area dependence of I-t' relations under conditions V_u=1, R_u=1, t_u=0.6, k=6, U_u=3 and ε_u=800, blue line (A=10 cm^2), red line (A=6 cm^2), black line (A=3 cm^2); (b) duration dependence of I-t' relations under conditions V_u =1, R_u =1, k =6, U_u =3, A_u=3 and ε_u =800, orange line (t_0=0.2 μs), magenta line (t_0=0.4 μs), black line (t_0=0.6 μs); (c) sign change of current under conditions R_u =1, k =0.2, U_u =3, A_u =3 and ε_u =300, blue line (V=0.75 V, t_0=0.25 μs), red line (V=1 V, t_0=0.2 μs); (d) duration dependence of a rectangular shape for I-t' relations under conditions V_u =1, R_u =1, k =3, U_u =3, A_u =3 and ε_u =300, blue line (t_0=1 μs) and red line (t_0=0.6 μs).*

4. Conclusions

In summary, in this work it is pointed out that Fermi surface energy of a material is position dependence, and accordingly uncover a new physical law as well as a physical effect in condensed materials, *i.e*, *Yuheng Zhang equation* and *Yuheng Zhang effect*. By investigations using this law and this effect, some new understandings of multi-physical properties of materials are gained: 1) materials experiencing strain gradient could present current-rectifying properties; 2) pure semiconductors with dramatic strain difference could be used as a new type of solar cell; 3) thermal expansion (contraction) and *Yuheng Zhang effect* contribute to thermoelectric power and Seebeck coefficient obviously; 4) *Yuheng Zhang effect* gives a new mechanism of electron-phonon interaction; 5) some crystalline defects and topological defects in materials, such as dislocations, Abrikosov vortices and so on, are often accompanied by a surrounding electric field and an electrical potential; 6) strain gradient can cause an electric polarization in dielectric materials; 7) the gravity induced electric field persists in the earth, which may be useful for earthquake research; 8) microscopic physical origin of flexoelectric effect, a challenge for more than half a century in the world, may be figured out by *Yuheng Zhang equation,* and the flexoelectric coefficients can be derived directly using this equation; 9) microscopic theory of shock polarization, another long-standing problem in the world, may be clarified in terms of *Yuheng Zhang equation*. In all, *Yuheng Zhang equation* offer people new understanding of electric properties of strained materials, and may find many application in multi-areas.

References

[1] A. W. Stepanow, Über den mechanismus der plastischen deformation, *Zs. Phys*. 81, 560 (1933).

[2] J. E. Caffin and T. L. Goodfellow, Electrical effects associated with the mechanical deformation of single crystals of alkali halides, *Nature*, 176, 878 (1955).

[3] G. E. Hauver, Shock Induced Polarization in Plastics. II. Experimental Study of Plexiglas and Polystyrene, *J. Appl. Phys.* 36, 2113-2118 (1965).

[4] V. N. Mineev and A. G. Ivanov, Electromotive force produced by shock compression of a substance, *Sov. Phys. Usp.*, 19, No. 5, 400-419 (1976).

[5] R. A. Graham, Shock-induced electrical activity in polymeric solids. a mechanically induced bond scission model, *The Journal of Physical Chemistry*, 83, No. 23, 3048-3056 (1979).

[6] Paul Harris, HenriNöel Presles, The shock induced electrical polarization of water, *J. Chem. Phys.* 77, 5157 (1982).

[7] A. I. Goncharov, S. P. Solovie, Shockk-induced polarization of materials, *Combustion*, *Explosion*, *and Shock Waves*, 40, No. 6, 658-662 (2004).

[8] Paul. Harris, Mechanism for the shock polarization of dielectrics, *J. Appl. Phys.* 36, No. 3, 739-741 (1965).

[9] J. Y. Wong, R. K. Linde, R. M. White, Electrical signals in dynamically stressed ionic crystals: a dislocation model, *J. Appl. Phys.* 40, No. 10, 4137-4145 (1969).

[10] F. E. Allison, Shock-induced polarization in plastics. I. theory, *J. Appl. Phys.* 36, No. 7, 2111-2113 (1965).

[11] R. J. Eichelberger and G. E. Hauver, in: Les ondes de detonation, P., 1961, p. 364.

[12] D. Hull, D. J. Bacon, Introduction to Dislocations (Pergamon, Oxford, 1994)

[13] D. B. Holt, B. G. Yacobi, Extended Defects in Semiconductors (Cambridge University Press, Cambridge, 2007)

[14] [14]. M. Reiche, M. Kittler, H. Uebensee, E. Pippel, S. Hopfe, Dislocations as native nanostructures-electronic properties, *Adv*. *Nano Res*. 2, 1 (2014).

[15] M. Reiche, M. Kittler, W. Erfurth, E. Pippel, K. Sklarek, H. Blumtritt, A. Haehnel, H. Uebensee, On the electronic properties of a single dislocation, *J. Appl*. *Phys*. 115, 194303 (2014).

[16] M. Reiche, M. Kittler, H. Ubensee, E. Pippel, A. Haehnel, S. Birner, Electronic properties of dislocations, *Appl*. *Phys*. *A* 122: 389 (2016).

[17] A. Hikata, C. Elbaum, B. Chick, R. Truell, Electrical-charge Study in Sodium Chloride During Plastic Deformation, *J. Appl. Phys*. 34, No. 8, 2154-2158 (1963).

[18] Frederick Seitz, Speculations on the Properties of The Silver Halide Crystals, *Rev. Mod. Phys.* 23, No. 4, 328-3532 (1951)

[19] R. J. Schwensfeir, C. Elbaum, Electric charge on dislocation arrays in sodium chloride, *J. Phys. Chem. Solids*, 28, 597-606 (1967).

[20] V. Nagarajan, C. L. Jia, H. Kohlstedt, R. Waser, I. B. Misirlioglu, S. P. Alpay, R. Ramesh, Misfit dislocations in nanoscale ferroelectric heterostructures, *Appl. Phys. Lett.* 86, 192910 (1-3) (2005).

[21] S. P. Alpay, I. B. Misirlioglu, V. Nagarajan, R. Ramesh, Can interface dislocations degrade ferroelectric properties? *Appl. Phys. Lett.* 85, No. 11, 2044-2046 (2004).

[22] Daesu Lee, Tae Won Noh, Giant flexoelectric effect through interfacial strain relaxation, *Phil. Trans. R. Soc. A* 370, 4944–4957 (2012).

[23] Yuanjie Huang, Yuheng Zhang Effect: Strain-induced electric effect in metals, *viXra*: 1707.0147 (2017).

[24] Holler, F. James; Skoog, Douglas A.; Crouch, Stanley R. Principles of Instrumental Analysis (6th ed.). Cengage Learning. (2007). p. 9.

[25] IUPAC Gold Book, definition of Galvani potential difference.

[26] Zhicheng Wang, Thermodynamics · Statistical Physics, 5th ed., Higher Education Press: Beijing, 2013, pp 145-148.

[27] Jenny Nelson, The Physics of Solar Cells (Yang Gao translate), Imperial College Press, United Kingdom, 2003 (Shanghai Jiao Tong University Press, 2011, pp 9.)

[28] Liangxiu Ye, Semiconductor Physics (part one), second edition, Higher Education Press, Beijing, 2007, pp 328.

[29] H. Joon Kim, S. Hoon Oh, and Hyun M. Jang, Thermodynamic theory of stress distribution in epitaxial Pb(Zr, Ti)O_3 thin films, *Appl. Phys. Lett.* 75, 3195 (1999).

[30] A. Haug, Theoretical Solid State Physics, Pergamon Press, Oxford, 1972.

[31] G. D. Mahan, Good Thermoelectrics, *Solid State Phys*. 51, (1998) 81-157.

[32] C. Kittel, Introduction to Solid State Physics, seventh ed., John Wiley and Sons, Singapore, (2004).

[33] P. Taylor and O. Heinonen, A Quantum Approach to Condensed Matter Physics Cambridge University Press, Cambridge, U.K., 2002.

[34] Jianwei Cai, G. D. Mahan, Effective Seebeck Coefficient for Semiconductors, *Phys. Rev. B* 74, 075201 (1-3) (2006).

[35] Philip Phillips, Advanced Solid State Physics [b], Westview Press (USA), (2003), p. 179.

[36] G. Gruner, The Dynamics of Charge-density Waves, *Rev. Mod. Phys.* 60, No. 4, 1129-1181 (1988).

[37] Ulrich Messerschmidt, Dislocation dynamics during plastic deformation (Springer Series in Materials Science 129), Springer, (2010), p. 42.

[38] Yuanjie Huang, Possible source of the earth's geomagnetic field, *viXra*: 1709.0024 (2017).

[39] K. X. Chen, Q. Dai, W. Lee, J. K. Kim, E. F. Schubert, J. Grandusky, M. Mendrick, X. Li, and J. A. Smart, Effect of dislocations on electrical and optical properties of n-type $Al_{0.34}Ga_{0.66}N$, *Appl. Phys. Lett.* 93, 192108 (2008).

[40] A. A. Allerman, M. H. Crawford, A. J. Fischer, K. H. A. Bogart, S. R. Lee, D. M. Follstaedt, P. P. Provencio, and D. D. Koleske, Growth and design of deep-UV (240–290nm) light emitting diodes using AlGaN alloys, *J. Cryst. Growth* 272, 227 (2004).

[41] Shakti Chauhan and Ashraf F. Bastawros, Probing thickness-dependent dislocation storage in freestanding Cu films using residual electrical resistivity, *Appl. Phys. Lett.* 93, 041901 (2008).

[42] R. P. Huebener, Dynamics of magnetic flux structures in superconductor, *Physics Reports* (Section C of Physics Letters), 13, No. 4, 143-189 (1974).

[43] https://en.wikipedia.org/wiki/Magnetic_pressure

[44] H. H. Wen, S. L. Li, Z. W. Zhao, H. Jin, Y. M. Ni, Z. A. Ren, G. C. Che and Z. X. Zhao, Magnetic relaxation and critical current density of the new superconductor MgB_2, *Supercond. Sci. Technol.* 15, 315–319 (2002).

[45] Haihu Wen, Flux dynamics and vortex phase diagram of cuprate superconductors, *Physics*, 35, No. 1, 16 (2006).

[46] C. S. Yadav, P. L. Paulose, Upper critical field, lower critical field and critical current density of $FeTe_{0.60}Se_{0.40}$ single crystals, *New Journal of Physics* 11, 103046 (2009).

[47] Sh. M. Kogan, Piezoelectric effect during inhomogeneous deformation and acoustic scattering of carriers in crystals, *Sov. Phys. Solid State* 5, 2069 (1964).

[48] A. K. Tagantsev, Piezoelectricity and flexoelectricity in crystalline dielectrics. *Phys. Rev. B* 34, 5883-5889 (1986).

[49] Wenhui Ma and L. Eric Cross, Observation of the flexoelectric effect in relaxor $Pb(Mg_{1/3}Nb_{2/3})O_3$ ceramics, *Appl. Phys. Lett.* 78, 2920 (2001).

[50] H. Lu, C.-W. Bark, D. Esque de los Ojos, J. Alcala, C. B. Eom, G. Catalan, and A. Gruverman, Mechanical writing of ferroelectric polarization, *Science*, 336, 59-61 (2012).

[51] Pavlo Zubko, Gustau Catalan, and Alexander K. Tagantsev, Flexoelectric effect in solids, *Annual Review of Materials Research*, Vol. 43: 387-421 (2013).

[52] S. H. Baek, H. W. Jang, C. M. Folkman, Y. L. Li, B. Winchester, J. X. Zhang, Q. He, Y. H. Chu, C. T. Nelson, M. S. Rzchowski, X. Q. Pan, R. Ramesh, L. Q. Chen and C. B. Eom, Ferroelastic switching for nanoscale non-volatile magnetoelectric devices, *Nature Materials*, 9, 309 (2010).

[53] D. Lee, A. Yoon, S. Y. Jang, J.-G. Yoon, J.-S. Chung, M. Kim, J. F. Scott, and T. W. Noh, Giant flexoelectric effect in ferroelectric epitaxial thin films, *Phys. Rev. Lett.* 107, 057602 (2011).

[54] H. W. Jang, A. Kumar, S. Denev, M. D. Biegalski, P. Maksymovych, C. W. Bark, C. T. Nelson, C. M. Folkman, S. H. Baek, N. Balke, C. M. Brooks, D. A. Tenne, D. G. Schlom, L. Q. Chen, X. Q. Pan, S. V. Kalinin, V. Gopalan, and C. B. Eom, Ferroelectricity in strain-free $SrTiO_3$ thin films, *Phys. Rev. Lett.* 104, 197601 (2010).

[55] Ronald K. Linde, William J. Murri, Donald G. Doran, Shock-induced electrical polarization of alkali halides, *J. Appl. Phys.* 37, No. 7, 2527-2532 (1966).

[56] Paul Harris, Electromechanical shock waves, Technical Report No. 4532, July (1973).

[57] S. A. Bordzilovskii, S. M. Karakhanov, V. V. Polyudov, Investigation of the EMF of certain metal pairs under shock compression, 480-483 (1972). (Novosibirsk. Translated from Fizika Goreniya i Vzryva, Vol. 8, No. 4, pp. 586-590, October-December, 1972. Original article submitted May 3, 1972.).

[58] A. Migault and J. Jacquesson, in: Symposium of High Dynamic Pressure, Pairs, 1967, p. 431.